Journal of Power Sources 327 (2016) 333–339

Contents lists available at ScienceDirect

Journal of Power Sources

journal homepage: www.elsevier.com/locate/jpowsour

Centrifugally-spun carbon microfibers and porous carbon microfibers as anode materials for sodium-ion batteries

Mahmut Dirican [a, b], Xiangwu Zhang [a, *]

[a] Fiber and Polymer Science Program, Department of Textile Engineering, Chemistry and Science, North Carolina State University, Raleigh, NC 27695-8301, USA

[b] Department of Materials Science and Nanotechnology Engineering, Abdullah Gül University, Kayseri 38080, Turkey

HIGHLIGHTS

- Centrifugal spinning is performed to fabricate porous carbon microfibers.
- Porous carbon microfibers are evaluated as anode material in sodium-ion batteries.
- Specific capacity of porous carbon microfibers at the 200th cycle is 242 mAh g^{-1}.
- Porous carbon microfibers show stable cycling performance of 89% over 200 cycles.

ARTICLE INFO

Article history:
Received 18 May 2016
Received in revised form
11 July 2016
Accepted 19 July 2016
Available online 26 July 2016

Keywords:
Sodium-ion battery
Centrifugal spinning
Porous carbon microfibers
Capacity retention
Coulombic efficiency

ABSTRACT

Natural abundance and low cost of sodium resources bring forward the sodium-ion batteries as a promising alternative to widely-used lithium-ion batteries. However, insufficient energy density and low cycling stability of current sodium-ion batteries hinder their practical use for next-generation smart power grid and stationary storage applications. Electrospun carbon microfibers have recently been introduced as a high-performance anode material for sodium-ion batteries. However, electrospinning is not feasible for mass production of carbon microfibers due to its complex processing condition, low production rate and high cost. Herein, we report centrifugal spinning, a high-rate and low-cost microfiber production method, as an alternative approach to electrospinning for carbon microfiber production and introduce centrifugally-spun carbon microfibers (CMFs) and porous carbon microfibers (PCMFs) as anode materials for sodium-ion batteries. Electrochemical performance results indicated that the highly porous nature of centrifugally-spun PCMFs led to increased Na^+ storage capacity and improved cycling stability. The reversible capacity of centrifugally-spun PCMF anodes at the 200th cycle was 242 mAh g^{-1}, which was much higher than that of centrifugally-spun CMFs (143 mAh g^{-1}). The capacity retention and coulombic efficiency of the centrifugally-spun PCMF anodes were 89.0% and 99.9%, respectively, even at the 200th cycle.

1. Introduction

Exploring clean and sustainable energy sources is very crucial for the human society because our world is facing ever-growing global warming and inevitable energy crisis. Since harvesting natural energy sources such as wind, solar and hydropower are mainly depend on environmental conditions, they must be efficiently stored during the energy sourcing pick time for use when needed [1–3]. Rechargeable batteries store the energy efficiently without greenhouse gas emission and have been considered as one of the most promising technologies for renewable energy storage [4,5]. Because of their distinguished features, including high energy density, durable cycling stability and good power performance, rechargeable lithium-ion batteries have been counted as the most preferred battery technology for portable devices and electric vehicles [6,7]. However, ever growing cost of lithium due to limited reserves of lithium element in the earth crust hinders the use of lithium-ion batteries for large-scale applications, such as smart power grids and stationary energy storage [3,8]. Nowadays, ambient temperature sodium-ion batteries are regarded as one of

* Corresponding author.
E-mail address: xiangwu_zhang@ncsu.edu (X. Zhang).

http://dx.doi.org/10.1016/j.jpowsour.2016.07.069
0378-7753/

the most promising alternatives to lithium-ion batteries for large-scale applications, due to the low cost and abundance of sodium resources [9,10]. However, insufficient energy density and poor cycling stability of current sodium-ion batteries prevent their practical implementation for advanced energy storage systems. The development of anode materials with enhanced capacity and cycling stability for sodium-ion batteries will be critically important for technological improvements on smart electric grids and stationary energy storage [11–13].

Discovering an appropriate anode material with adequate Na-insertion capacity and cycling capability is extremely crucial because the radius of Na ions (~1.09 A) is much larger than that of Li ions (~0.74 A), which makes intercalation and deintercalation processes of sodium-ion batteries quite distinctive than those of lithium-ion batteries [14,15]. Graphite is a good example to indicate the importance of this matter. As pointed out in many similar studies, although graphite is a widely-used anode material in current lithium-ion batteries, it can barely store sodium ions in its layer structure [16]. On the other hand, hard carbon has been reported as a convenient anode for Na insertion because of its disordered nature and wide interlayer distance [17]. Recently, transition metals (e.g., tin, antimony, and germanium) and their oxides, which intercalate Na ions based on conversion mechanism and exhibit much higher capacities than that of graphite, have been studied as potential anode materials for Na-ion batteries [18,19]. However, insertion of sodium ions into these anodes results in large volumetric change, which leads to severe pulverization and demolishing of electrical contact between the active material and carbon conductor [15,20]. These drawbacks bring together intense capacity loss during the sodium insertion and extraction processes. Currently, reducing the size of active materials into the nanoscale range is considered as one of the most efficient methods for eliminating the volume change problem [20,21].

Recently, micro- and nanostructured carbonaceous materials, such as nanospheres, nanotubes, and microfibers, have been widely examined as anode material for lithium-ion and sodium-ion batteries [22]. Among these micro- and nanostructured carbonaceous anodes, carbon microfibers (CMFs) and CMF-based composites have drawn great attention due to their high cyclability and rate capability features. Most CMFs and CMF-based composites introduced for lithium-ion and sodium-ion batteries have been synthesized through the electrospinning of polymer precursor fibers and subsequent carbonization processes [18,22,23]. Although the electrospinning method is versatile for altering fiber diameter and morphology, it is not considered an appropriate approach for mass production of CMFs because of its low production rate, high cost, complex processing condition and safety concern [24,25]. In recent years, centrifugal spinning has gained great attention as a low-cost and highly efficient alternative method for synthesizing microfibers for large-scale applications [26]. To this end, centrifugal spinning has been widely investigated to fabricate both polymeric and inorganic micro and nanofibers for different applications such as mechanical enforcement, tissue engineering, and energy storage [27–30]. Herein, we report the preparation of CMFs as an anode material for sodium-ion batteries by the centrifugal spinning of polyacrylonitrile (PAN) precursor, followed by carbonization. To increase the active sites for Na storage, porous carbon microfibers (PCMFs) were also fabricated by the centrifugal spinning and carbonization of a mixture of PAN and polymethyl methacrylate (PMMA) precursors. During the carbonization process, PAN was pyrolyzed to carbon while PMMA was thermally degraded to form nanoscale pores in the resultant carbon microfiber matrix. Electrochemical performance studies reveal that the high porosity of centrifugally-spun PCMFs resulted in increased Na^+ storage capacity and improved cycling stability. At the 200th cycle, the reversible capacity of centrifugally-spun PCMF anodes was 242 mAh g^{-1}, which was much higher than that of centrifugally-spun CMFs (143 mAh g^{-1}). The capacity retention and coulombic efficiency of the centrifugally-spun PCMF anodes were 89.0% and 99.9%, respectively, even at the 200th cycle. These results demonstrate that centrifugal spinning is a promising alternative to electrospinning in fabricating PCMF anode materials with increased Na^+ storage capacity and improved cycling stability.

2. Experimental

2.1. Chemicals

Polyacrylonitrile (PAN, Pfaltz & Bauer Inc., 150,000 g mol^{-1}), polymethyl methacrylate (PMMA, Aldrich, 120,000 g mol^{-1}) and *N*,*N*-dimethylformamide (DMF, Aldrich) were used without further purification.

2.2. Centrifugal spinning of PAN and PAN/PMMA precursor fibers

PAN and PAN/PMMA precursor fibers were fabricated by centrifugal spinning of PAN and PAN/PMMA blend solutions, respectively. To this end, two different DMF solutions of 15 wt% PAN and 15 wt% PAN/PMMA blend (PAN-to-PMMA mass ratio = 1/1) were prepared and mechanically stirred for 24 h at 70 °C. PAN and PAN/PMMA precursor fibers were fabricated by using a lab-scale centrifugal spinning device. Fig. 1 shows the schematic illustration of the centrifugal spinning apparatus and the fabrication process of PAN and PAN/PMMA precursor fibers. The centrifugal spinning device used in this study was composed of a perforated Teflon spinneret placed in the center of the spinning apparatus, a motor connected to the spinneret to provide high-speed rotation, a speed controller to tune the rotational speed of the spinneret, and a series of fiber collector rods placed radially in the outer perimeter of the Teflon spinneret. The spinneret was in a cylindrical shape with 1.5 cm in radius and 2 cm in height, and it had two nozzles with inner diameter of 0.4 mm on the sidewall. The distance from the spinneret to rod collectors was 10 cm. For the fabrication of centrifugally-spun PAN and PAN/PMMA precursor fibers, PAN/DMF and PAN/PMMA/DMF solutions were loaded into the Teflon spinneret and the rotation was started. Spinning process of PAN/DMF and PAN/PMMA/DMF solutions was performed with a rotational speed of 4000 rpm at room temperature. Centrifugally-spun precursor fibers were collected on aluminum rods placed around the spinneret.

2.3. Synthesis of nonporous and porous carbon microfibers

CMFs and PCMFs were prepared by the thermal treatment of centrifugally-spun PAN and PAN/PMMA precursor fibers. During preparation, PAN and PAN/PMMA fibers were initially stabilized in air atmosphere at 280 °C for 5.5 h with a heating rate of 5 °C min^{-1} and further carbonized at 700 °C for 2 h in argon environment with a heating rate of 2 °C min^{-1}, during which PAN was converted to carbon while PMMA was thermally decomposed to form nanoscale pores in the carbon matrix.

2.4. Structure characterization

The morphology of centrifugally-spun CMFs and PCMFs was investigated by field emission scanning electron microscope (FE-SEM, FEI Verios 460L) and scanning transmission electron microscope (STEM, JEOL 2000FX). The structure of microfibers was examined by Fourier transform infrared spectroscopy (FTIR, Nicolet Nexus 470) and wide angle X-ray diffraction (WAXD, Rigaku

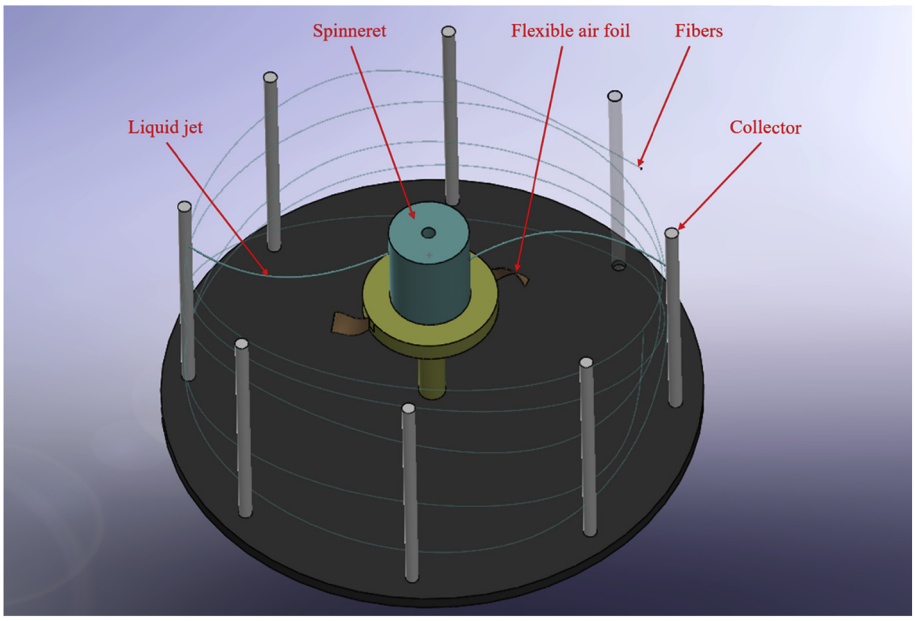

Fig. 1. Schematic illustration of centrifugal spinning of PAN and PAN/PMMA precursor fibers.

Smartlab).

2.5. Electrochemical evaluation

The electrochemical properties of centrifugally-spun CMFs and PCMFs were examined using CR 2032-type coin cells. The working electrodes were prepared by a mixed slurry of 80% centrifugally-spun CMFs and PCMFs, 12% carbon black, and 8% sodium-alginate binder dissolved in deionized water. The as-prepared slurry was coated onto a copper foil as current collector and dried at 80 °C for 12 h. Then thickness of each electrode was around 1.5 mm. The dried electrodes were punched into circular disks with 0.5 inches in diameter. Pure sodium metal (Aldrich) was used as the counter electrode, and glass fiber mat (Whatman) was used as the separator. The electrolyte was prepared by dissolving 1 M sodium perchlorate ($NaClO_4$) in ethylene carbonate (EC) and dimethyl carbonate (DMC) (1:1 in volume). Coin cells were assembled in a high-purity argon-filled glove box. Cyclic voltammetry (CV) tests were conducted using Reference 600 Potentiostat/Galvanostat/ZRA (GAMRY). Galvanostatic charge-discharge tests were conducted at constant current density of 50 mA g^{-1} with cut-off potentials of 0.01 and 3.00 V using LAND-CT 2001A battery tester. The rate performance was tested using the same instrument at current densities of 50, 100, 200, 400, and 800 mA g^{-1}. The overall reproducibility of the electrochemical testing results was affirmed by conducting all measurements on at least fifteen samples for each electrode.

3. Results and discussion

3.1. Morphology and structure

PAN and PAN/PMMA precursor fibers were first fabricated by centrifugal spinning. The morphology of centrifugally-spun PAN and PAN/PMMA precursor fibers was examined by SEM. As shown in Fig. 2(A–D), the surface morphologies of both PAN and PAN/PMMA precursor fibers are similar. Both precursor fibers demonstrate smooth surface without visible bead formation. It is seen from the SEM images of PAN and PAN/PMMA precursor fibers that the diameters of both PAN and PAN/PMMA precursor fibers are very similar.

CMFs and PCMFs were prepared by the thermal treatment of centrifugally-spun PAN and PAN/PMMA precursor fibers. Fig. 2(E–H) shows the plane-viewed and cross-sectional SEM images of centrifugally-spun CMFs and PCMFs. It is seen from the plane-viewed SEM images that both centrifugally-spun CMFs and PCMFs exhibit continuous fibrous morphology without obvious bead formation (Fig. 2E and G). On the other hand, the cross-sectional SEM image of PCMFs demonstrates the formation of a vast quantity of internal pores and surface roughness (Fig. 2H), which cannot observed for CMFs (Fig. 2F). The porous structure of PCMFs was created by the decomposition of PMMA during the thermal treatment process. TEM images of centrifugally-spun CMFs and PCMFs are also used as complimentary evidence to show the porous nature of the PCMFs (Fig. 3). It is seen that a multi-channel porous architecture was formed in centrifugally-spun PCMFs.

The X-ray diffraction (XRD) patterns of centrifugally-spun CMFs and PCMFs are presented in Fig. 4(A). It is seen that both CMFs and PCMFs exhibit a broad and weak diffraction peak at around $2\theta = 25°$, which could be indexed as the (002) planes of disordered carbon structure, indicating the amorphous nature of CMFs and PCMFs [31,32]. The interlayer spacing (d_{002}) of PCMFs is calculated to be ~0.36 nm, which is higher than that of graphite (0.336 nm). On the other hand, interlayer spacing (d_{002}) of CMFs was ~0.35 nm. Turbostratic structure and large interlayer spacing between graphene sheets of carbonaceous anodes are essential for the reversible sodium ion storage.

The structural evolution of centrifugally-spun CMFs and PCMFs was also investigated by Raman spectroscopy. Fig. 4(B) shows the Raman spectra of centrifugally-spun CMFs and PCMFs. For both CMFs and PCMFs, the characteristic carbon peaks of D-band (1360 cm^{-1}), representing the disordered sp^2 phase, and G-band (1582 cm^{-1}), indicating the in-plane stretching vibration mode of E_{2g} graphite, can be observed [33,34]. The relative intensity ratio (i.e., *R*-value) of D-band to G-band demonstrates the degree of disorder in the structure. Typically, a higher *R*-value indicates a higher degree of disorder within the carbon structure [33,35]. As demonstrated in Fig. 4(B), the *R*-values of the centrifugally-spun

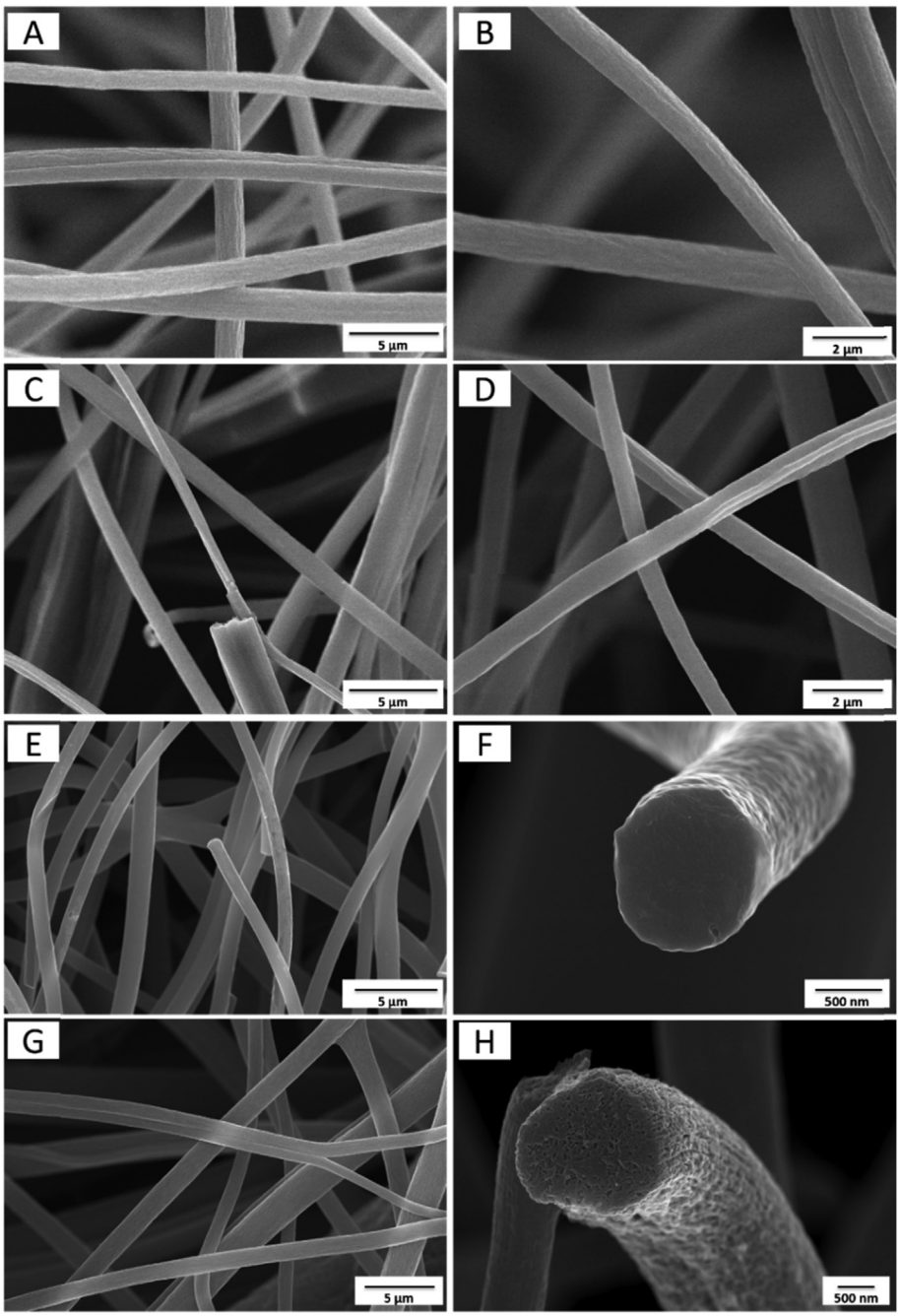

Fig. 2. SEM images of centrifugally-spun PAN microfibers (A and B), PAN/PMMA microfibers (C and D), and corresponding CMFs (E and F) and PCMFs (G and H), respectively.

CMFs and PCMFs are 0.97 and 1.12, respectively. This reveals that centrifugally-spun PCMFs are more disordered than nonporous CMFs.

3.2. Electrochemical performance

Cyclic voltammetry (CV) and galvanostatic charge-discharge tests were carried out to evaluate the electrochemical performance of centrifugally-spun CMFs and PCMFs for use as anodes in sodium-ion batteries. Cyclic voltammetry (CV) tests were performed between 0 and 3 V with a scan rate of 0.1 mV s^{-1} to reveal the electrochemical behavior of CMFs and PCMFs, and the results are shown in Fig. 5. For CMFs, three-cathodic peaks are observed at around 1.28, 0.50, and 0 V during the first scan (Fig. 5(A)). The first peak at 1.28 V is attributed to the reaction of sodium ions on the carbon microfiber surface [36]. This peak is preserved in the subsequent cycles even though it becomes more prominent, demonstrating that the reaction is partially reversible. The irreversible peak at 0.50 V is ascribed to the decomposition of sodium electrolyte and subsequent solid electrolyte interphase (SEI) formation [16]. The third cathodic peak located at around 0 V corresponds to the insertion of sodium ions into porous carbon [37]. In the anodic scan of PCMFs, a small peak indexed at around 0.2 V in the first and subsequent cycles is ascribed to the extraction of sodium ions from porous carbon [36]. Comparing Fig. 5(A) and (B), it is observed that the CV behaviors of PCMFs are similar to that of CMFs excepting

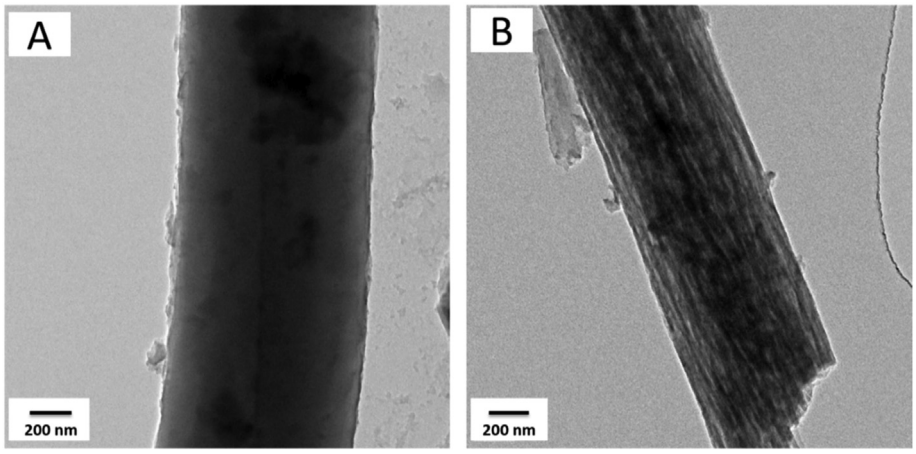

Fig. 3. TEM images of centrifugally-spun CMFs (A) and PCMFs (B).

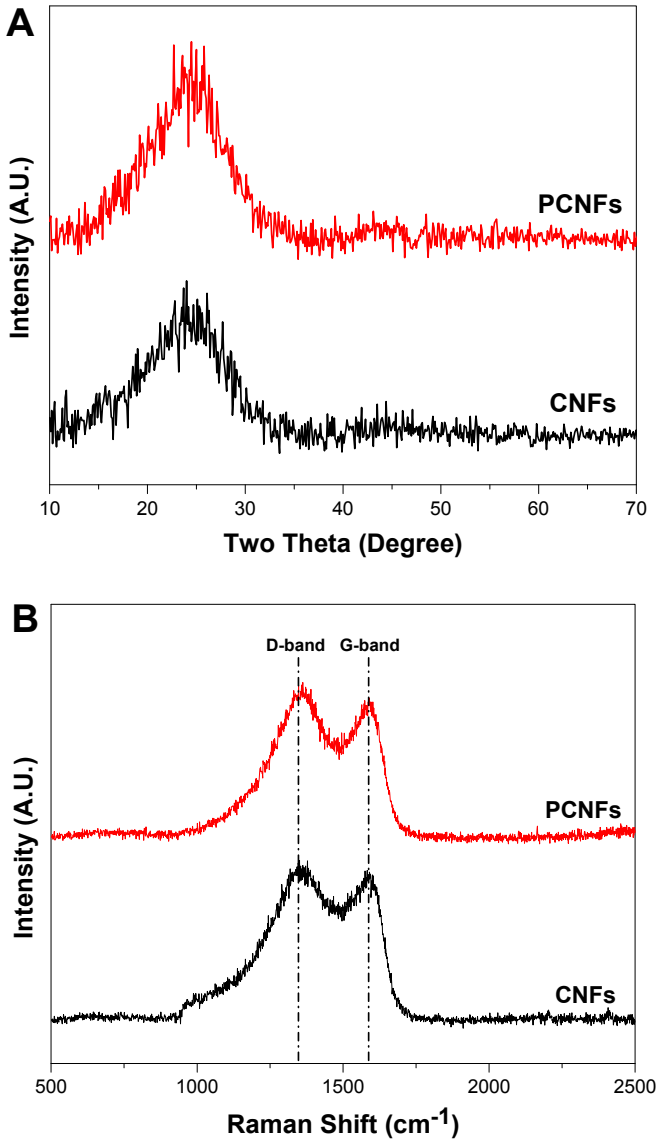

Fig. 4. WAXD patterns (A) and Raman spectra (B) of centrifugally-spun CMFs and PCMFs.

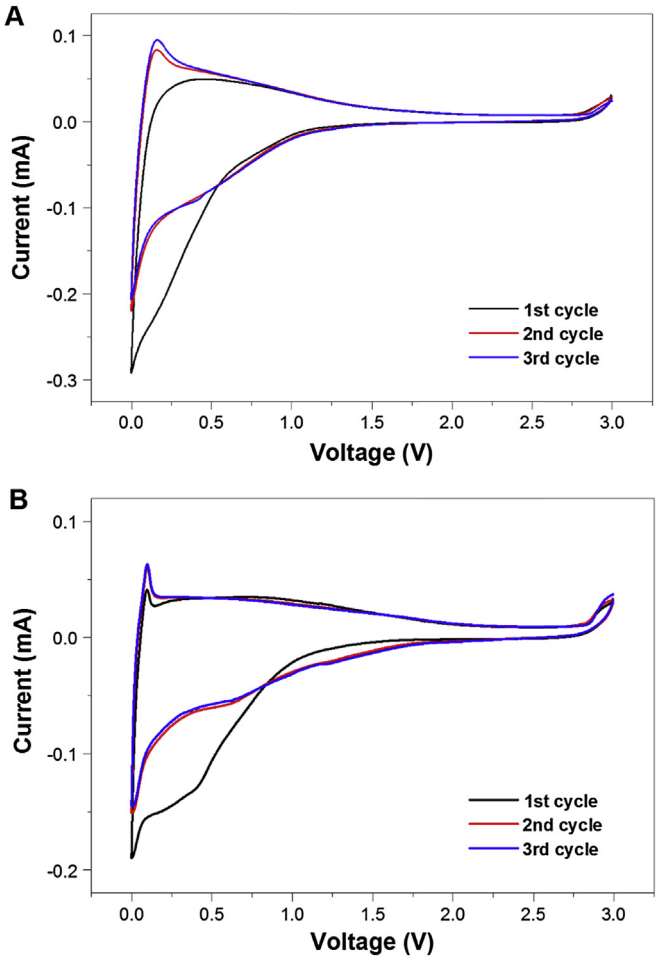

Fig. 5. Cyclic voltammetry curves of centrifugally-spun CMFs (A) and PCMFs (B).

small fluctuations. The decreases of the area under the CV curve after the first scan corresponds to the irreversible capacity loss in the initial charge-discharge process, which is mainly ascribed to the formation of SEI film on the electrode surface. However, the CV curves in the subsequent cycles remain almost the same, revealing good electrochemical reversibility of the CMFs and PCMFs

electrodes.

Galvanostatic charge-discharge measurements were conducted between 0.01 and 3.0 V at a constant current density of 50 mA g^{-1} to investigate the electrochemical performance of centrifugally-spun CMFs and PCMFs. Fig. 6 shows the galvanostatic charge-discharge profiles for the first, second and fifth cycles of CMFs and PCMFs. It is observed from Fig. 6 that a sloping-voltage region at higher voltages and a voltage plateau at lower potentials can be identified in the first discharge curves of both CMFs and PCMFs. The low-voltage plateau represents the sodium insertion into the structurally disordered carbon microfibers. On the other hand, the sloping region on the first discharge curve could be attributed to various insertion mechanisms such as adsorption of Na^+ ions on both sides of single graphene layers or formation of partly reversible bonds of sodium with C–H group [38].

From Fig. 6, it is also seen that PCMFs exhibit higher initial sodium storage capability than CMFs. At the first cycle, the discharge capacities are 227 and 469 mAh g^{-1}, respectively, for CMFs and PCMFs. At the second cycle, the discharge capacities of CMFs and PCMFs reduce to 183 and 297 mAh g^{-1}, respectively. Electrochemical test results demonstrate that, compared with CMFs, the highly porous nature of PCMFs leads to higher Na^+ insertion capacities. Higher charge-discharge capacity of the PCMFs is attributed to the beneficial structural properties of these fibers such as short diffusion pathway for both sodium ions and electrons, numerous active sites for charge transfer reaction and good electrical conductivity acquired by well interconnected neighboring microfibers. During the initial cycle, both CMFs and PCMFs exhibit relatively high irreversible capacities due to the electrolyte decomposition and solid electrolyte interphase (SEI) formation. The first-cycle coulombic efficiencies of CMFs and PCMFs are 77.5% and 58.0%, respectively. The coulombic efficiencies of CMFs and PCMFs increase to 93.0%, and 97.7%, respectively, at the fifth cycle.

The cycling performance of CMFs and PCMFs was evaluated at a constant current density of 50 mA g^{-1} and results are demonstrated in Fig. 7. The capacity of CMFs at the 200th cycle is around 143 mAh g^{-1}, corresponding to a capacity retention of 80.6%. CMFs also exhibits a high coulombic efficiency of 99.9% at the 200th cycle. On the other hand, the capacity of PCMFs is around 242 mAh g^{-1} at the 200th cycle, with a corresponding capacity retention of 89.0%, which is much higher than that of CMFs. PCMFs also demonstrate a high coulombic efficiency of 99.8% at the 200th cycle. Cycling performance results demonstrate that the porous nature of PCMFs not only increases Na^+ storage capacity but also ensures better cycling stability. It should also be noticed that for both CMFs and PCMFs, the capacity loss mainly occurs in the first 30 cycles, after which the coulombic efficiency approaches approximately 98.0% or higher.

The rate capability of CMFs and PCMFs was investigated under different current densities and the results are demonstrated in Fig. 8. The average charge capacities of CMFs are around 155, 120, 82, 47, and 27 mAh g^{-1}, respectively, at 50, 100, 200, 400, and 800 mA g^{-1} (Fig. 8(A)). The coulombic efficiency does not exhibit prominent change as the current density increases and it remains as high as 99.6% even at the highest current density of 800 mA g^{-1}. After undergoing cycles at higher current densities, the charge capacity value returns to 147 mAh g^{-1} under a reduced current density of 50 mAh g^{-1}. On the other hand, the average charge capacities of PCMFs are around 252, 224, 200, 172, and 138 mAh g^{-1}, respectively, at 50, 100, 200, 400, and 800 mA g^{-1} (Fig. 8(B)). The charge capacity value returns to 241 mAh g^{-1} under a reduced current density of 50 mAh g^{-1} after ongoing cycles at higher current densities. This charge capacity (241 mAh g^{-1}) is very close to the initial charge capacity, which also indicates the good rate capability of PCMFs. Similar to CMFs, the coulombic efficiency of PCMFs does not show remarkable change as the current density increases and it remains at 99.9% even at the highest current

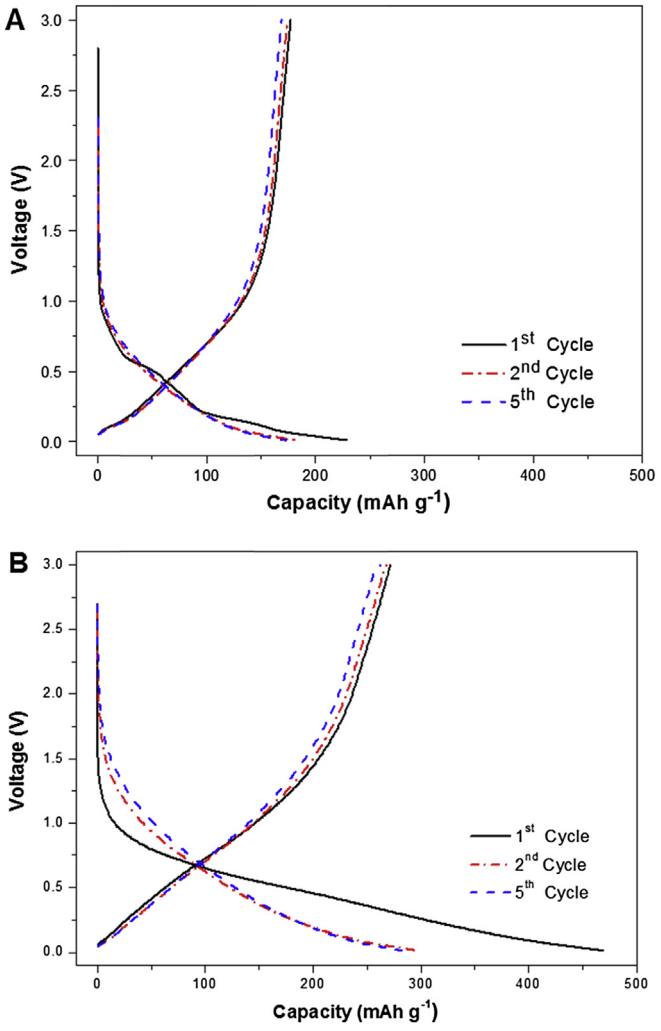

Fig. 6. Galvanostatic charge-discharge profiles of centrifugally-spun CMFs (A) and PCMFs (B).

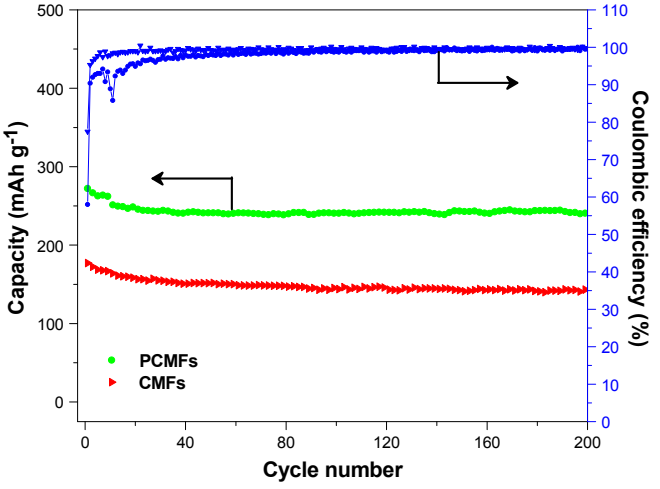

Fig. 7. Cycling performance and coulombic efficiencies of centrifugally-spun CMFs and PCMFs.

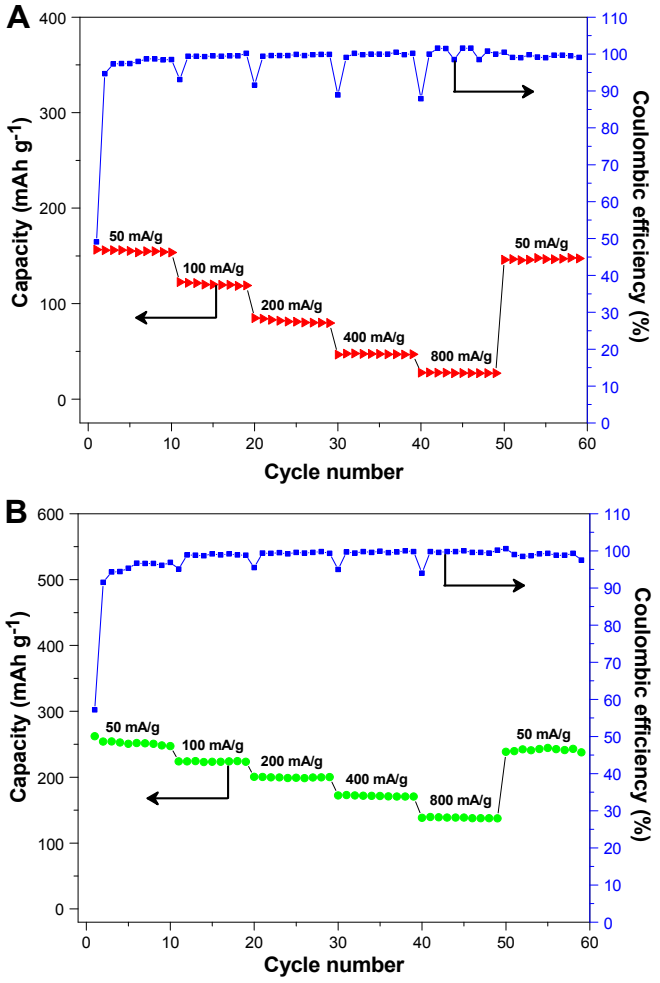

Fig. 8. Rate capabilities of centrifugally-spun CMFs (A) and PCMFs (B) cycled at different current densities.

density of 800 mA g^{-1}. These electrochemical results demonstrate that centrifugally-spun PCMFs are a promising anode material for sodium-ion batteries in high rate applications.

4. Conclusions

CMFs and PCMFs were fabricated by centrifugal spinning of PAN and PAN/PMMA precursor solutions followed by subsequent two-step thermal treatment, oxidation and carbonization, and were investigated as anode materials for sodium-ion batteries. The PMMA ingredient of PAN/PMMA precursor fibers led to the formation of highly porous structure for PCMFs, which helped ensure the increased Na^+ storage capacity and improved cycling stability when used in sodium-ion batteries. Electrochemical test results demonstrated that the capacity of PCMFs was around 242 mAh g^{-1} at the 200th cycle, which was much higher than that of CMFs (143 mAh g^{-1}). The capacity retention and coulombic efficiency of PCMFs were 89.0% and 99.9%, respectively, at the 200th cycle. Therefore, it was demonstrated that centrifugally-spun PCMFs are promising anode candidate for next-generation sodium-ion batteries.

Acknowledgments

This study was supported by National Science Foundation under Award Number CMMI-1231287.

References

[1] M.-D. Slater, D. Kim, E. Lee, C.-S. Johnson, Adv. Funct. Mater. 23 (2013) 947–958.
[2] H.-D. Yoo, E. Markevich, G. Salitra, D. Sharon, D. Aurbach, Mater. Today 17 (2014) 110–121.
[3] Y. Ge, H. Jiang, J. Zhu, Y. Lu, C. Chen, Y. Hu, Y. Qiu, X. Zhang, Electrochim. Acta 157 (2015) 142–148.
[4] N. Liu, H. Wu, M.-T. McDowell, Y. Yao, C. Wang, Y. Cui, Nano Lett. 12 (2012) 3315–3321.
[5] L. Ji, O. Toprakci, M. Alcoutlabi, Y. Yao, Y. Li, S. Zhang, B. Guo, Z. Lin, X. Zhang, ACS Appl. Mater. Interfaces 4 (2012) 2672–2679.
[6] X. Yu, S. Yang, B. Zhang, D. Shao, X. Dong, Y. Fang, Z. Li, H. Wang, J. Mater. Chem. 21 (2011) 12295–12302.
[7] M. Dirican, M. Yanilmaz, K. Fu, O. Yildiz, H. Kizil, Y. Hu, X. Zhang, J. Electrochem. Soc. 161 (2014) A2197–A2203.
[8] L. Wu, D. Buchholz, D. Bresser, L.G. Chagas, S. Passerini, J. Power Sources 251 (2014) 379–385.
[9] M.-K. Datta, R. Epur, P. Saha, K. Kadakia, S.-K. Park, P.-N. Kumta, J. Power Sources 225 (2013) 316–322.
[10] Y. Kim, Y. Kim, A. Choi, S. Woo, D. Mok, N.-S. Choi, Y.-S. Jung, J.-H. Ryu, S.-M. Oh, K.-T. Lee, Adv. Mater. 26 (2014) 4139–4144.
[11] P.-K. Dutta, U.-K. Sen, S. Mitra, RSC Adv. 4 (2014) 43155–43159.
[12] J. Song, Z. Yu, M.-L. Gordin, S. Hu, R. Yi, D. Tang, T. Walter, M. Regula, D. Choi, X. Li, Nano Lett. 14 (2014) 6329–6335.
[13] Y. Denis, P.-V. Prikhodchenko, C.-W. Mason, S.-K. Batabyal, J. Gun, S. Sladkevich, A.-G. Medvedev, O. Lev, Nat. Commun. 4 (2013) 2922.
[14] L. Fan, J. Zhang, J. Cui, Y. Zhu, J. Liang, L. Wang, Y. Qian, J. Mater. Chem. A 3 (2015) 3276–3280.
[15] Y.-N. Ko, Y.-C. Kang, Chem. Commun. 50 (2014) 12322–12324.
[16] Z. Wang, L. Qie, L. Yuan, W. Zhang, X. Hu, Y. Huang, Carbon 55 (2013) 328–334.
[17] A. Ponrouch, A. Goñi, M.-R. Palacín, Electrochem. Commun. 27 (2013) 85–88.
[18] L. Wu, X. Hu, J. Qian, F. Pei, F. Wu, R. Mao, X. Ai, H. Yang, Y. Cao, Energy Environ. Sci. 7 (2014) 323–328.
[19] D. Su, C. Wang, H. Ahn, G. Wang, Phys. Chem. Chem. Phys. 15 (2013) 12543–12550.
[20] Y. Zhu, X. Han, Y. Xu, Y. Liu, S. Zheng, K. Xu, L. Hu, C. Wang, ACS Nano 7 (2013) 6378–6386.
[21] L. Xiao, Y. Cao, J. Xiao, W. Wang, L. Kovarik, Z. Nie, J. Liu, Chem. Commun. 48 (2012) 3321–3323.
[22] J. Zhu, C. Chen, Y. Lu, Y. Ge, H. Jiang, K. Fu, X. Zhang, Carbon 94 (2015) 189–195.
[23] M. Dirican, O. Yildiz, Y. Lu, X. Fang, H. Jiang, H. Kizil, X. Zhang, Electrochim. Acta 169 (2015) 52–60.
[24] M.-R. Badrossamay, H.-A. McIlwee, J.-A. Goss, K.-K. Parker, Nano Lett. 10 (2010) 2257–2261.
[25] Y. Lu, K. Fu, S. Zhang, Y. Li, C. Chen, J. Zhu, M. Yanilmaz, M. Dirican, X. Zhang, J. Power Sources 273 (2015) 502–510.
[26] Y. Lu, Y. Li, S. Zhang, G. Xu, K. Fu, H. Lee, X. Zhang, Eur. Polym. J. 49 (2013) 3834–3845.
[27] R. Weitz, L. Harnau, S. Rauschenbach, M. Burghard, K. Kern, Nano Lett. 8 (2008) 1187–1191.
[28] H. Jiang, Y. Ge, K. Fu, Y. Lu, C. Chen, J. Zhu, M. Dirican, X. Zhang, J. Mater. Sci. 50 (2015) 1094–1102.
[29] B. Weng, F. Xu, A. Salinas, K. Lozano, Carbon 75 (2014) 217–226.
[30] L. Ren, V. Pandit, J. Elkin, T. Denman, J.-A. Cooper, S.-P. Kotha, Nanoscale 5 (2013) 2337–2345.
[31] K. Fu, L. Xue, O. Yildiz, S. Li, H. Lee, Y. Li, G. Xu, L. Zhou, P.D. Bradford, X. Zhang, Nano Energy 2 (2013) 976–986.
[32] L. Ji, X. Zhang, Carbon 47 (2009) 3219–3226.
[33] Y.-S. Ding, W.-N. Li, S. Iaconetti, X.-F. Shen, J. DiCarlo, F.-S. Galasso, S.-L. Suib, Surf. Coat. Technol. 200 (2006) 3041–3048.
[34] L. Su, Z. Zhou, M. Ren, Chem. Commun. 46 (2010) 2590–2592.
[35] C. Kim, S.-H. Park, J.-I. Cho, D.-Y. Lee, T.-J. Park, W.-J. Lee, K.-S. Yang, J. Raman Spectrosc. 35 (2004) 928–933.
[36] J. Liu, H. Liu, T. Yang, G. Wang, M.-O. Tade, Chin. Sci. Bull. 59 (2014) 2186–2190.
[37] L. Fu, K. Tang, K. Song, P.-A. van Aken, Y. Yu, J. Maier, Nanoscale 6 (2014) 1384–1389.
[38] P. Thomas, D. Billaud, Electrochim. Acta 47 (2002) 3303–3307.